

ARTICLE

Using SERS and Electrochemical Melting to Discriminate *Yersinia Pestis* from *pseudotuberculosis* Based on Single Nucleotide Polymorphisms within Unpurified PCR Amplicons.

Cite this: DOI: 10.1039/x0xx00000x

Received 00th January 2012,
Accepted 00th January 2012

DOI: 10.1039/x0xx00000x

www.rsc.org/

E. Papadopoulou,^a S. A Goodchild,^b D. W Cleary,^b S. Weller,^b M. R Stubberfield,^b N. Gale,^c T. Brown^d and P.N Bartlett^{*a}

The development of sensors for the detection of pathogen-specific DNA including relevant species/strain level discrimination is critical in molecular diagnostics with major impacts in areas such as bioterrorism and food safety. Herein, we use electrochemically driven denaturation monitored by SERS to target single nucleotide polymorphism (SNP) that distinguish DNA extracted from the highly pathogenic *Yersinia pestis* bacterium, the causative agent of the systemic, invasive disease commonly known as plague, from that extracted from *Y. pseudotuberculosis*. Two assays targeting SNPs have been successfully achieved in 262 and 251 base pairs fragments using the unpurified PCR products. For the 251bp fragment that had a single base mismatch in the middle of the long PCR amplicon, three different probes were used to successfully detect three different combinations of mismatches. Conducting the electrochemical experiments at 10 °C resulted in greater discrimination. Replicated data were collected and analysed for each duplex on different days, using different batches of PCR product and different SSV substrates. Despite the variability introduced by these differences, the assays are shown to be reliable and robust providing a new platform for strain discrimination using unpurified PCR samples.

Introduction

The development of low cost, reliable and sensitive methods for detection of the presence of harmful bacteria in environmental,¹ food² or diagnostic samples including relevant species/strain level discrimination is a high priority objective to ensure that early diagnosis and treatment of infections can be implemented.³ Even though traditional immunological assays have been widely used for the detection of pathogens, it has been shown that the detection of pathogen-specific DNA is more specific, sensitive and less complex.⁴

Well-developed nucleic acid amplification and detection technologies such as Polymerase Chain Reaction (PCR) are robust and sensitive^{5, 6} and are widely used for detection of DNA from bacterial species of interest. PCR alone may not however be able to provide detailed species/strain level information in cases where pathogenic and non-pathogenic species of organism are highly similar in DNA sequence. Modern sequencing techniques are therefore frequently used to provide the resolution required to accurately type organisms.³ Sequencing technologies are however subject to high logistical, reagent and time burdens in order to provide the desired results. Lower burden options that provide a bridge between these two

technology areas include DNA-hybridisation based biosensors. Simple DNA hybridisation techniques can be coupled to PCR amplification (to increase the concentration of the target sequence prior to analysis), followed by a determination of the level of homology of the DNA to specific known sequences through hybridisation to probes within the biosensor. These biosensors can be based on optical methods such as fluorescence⁷⁻⁹ or surface enhanced Raman spectroscopy (SERS),¹⁰⁻¹³ electrochemical methods¹⁴ or enzyme amplification approaches.¹⁵ Electrochemical DNA-based biosensors are very promising, however only a few authors have reported DNA detection of PCR-amplified DNA that retain a full length DNA amplicon in unpurified PCR buffer¹⁶⁻¹⁸ while most of the reports have concentrated on the detection of short synthetic oligonucleotides. Mascini *et al.* have, for example, reported an electrochemical DNA sensor coupled with PCR amplification of a 244 base pair (bp) DNA product extracted from human blood for the detection of apolipoprotein E polymorphism.¹⁶ The DNA hybridization was monitored by chronopotentiometric stripping analysis. Ozsoc *et al.* reported an electrochemical genosensor for the detection of mutations from PCR amplicons using the intrinsic guanine signal and differential pulse voltammetry.^{17, 19} A drawback of this

approach is the need of high potentials to detect the oxidation of guanine. The same group reported the detection of influenza B virus from PCR samples using a redox active intercalator combined with differential pulse voltammetry.²⁰

Surface enhanced Raman spectroscopy (SERS) is an alternative fast-growing technique which can be used for the detection of DNA hybridization due to its ability to produce molecule specific vibrational spectra.^{21, 22} SERS-based DNA biosensors have been extensively reported,²³⁻²⁷ although only a few assays have used DNA extracted from biological samples.²⁸ A chromophore is usually attached to the DNA sequence which provides an enhanced distinct signal when the DNA is in close proximity to a SERS active metal surface. Faulds *et al.* demonstrated the multiplex detection of three PCR products (99-162 bp sequences) upon the reduction of the SERS signal obtained from a dye-labelled probe sequences following hybridization to their complementary targets. They showed discrimination between nonsense and complementary DNA.²⁹ *Staphylococcus epidermidis* was also detected using a SERS sensor coupled with PCR utilizing the higher affinity of single stranded DNA for the metal surface than double stranded DNA.¹¹ A PCR product from *Chlamydia trachomatis* was detected using a bead-based assay and SERS.³⁰ PCR free methods have also been reported for the detection of specific DNA sequences from biological samples utilizing array-format SERS sandwich assays.^{28, 31} The main drawback of these methods is that they are based on a hybridization event which makes the detection of a single mutation in long PCR amplicons very difficult.

In this article we use an electrochemically driven differential denaturation method monitored by SERS to detect and discriminate DNA sequences. In this method a DNA probe strand is immobilised on an ordered sphere segment void (SSV) Au surface.³² The SSV surface is designed to give a large and reproducible SERS enhancement.³³⁻³⁶ The target DNA strand, amplified by PCR and labelled with a Raman active dye, is hybridised to the surface bound probe. Upon application of an increasing negative potential the dsDNA denatures and the denaturation is monitored by following the intensity of the Raman signal from the labelled target DNA.³⁷⁻³⁹ Electrochemical melting curves, constructed by plotting the SERS intensity against the electrode potential, are then used to discriminate DNA sequences based on differences in the stability of the dsDNA.⁴⁰ Hence, we are not only able to detect specific DNA sequence but most importantly we can discriminate DNA sequences that vary by a single nucleotide, i.e. single nucleotide polymorphism (SNP). This methodology has been successfully used to differentiate mutations between wild type, a single point mutation (1653C/T), and a triple deletion (Δ F 508) in the cystic fibrosis trans-membrane regulator gene using both synthetic oligonucleotides and unpurified PCR products,^{39, 41} and to discriminate between polymorphic repeat sequences of the D16S539 locus using the unpurified PCR products.⁴²

In the current study we expand the work to explore the limits of this approach for discriminating phylogenetically informative polymorphisms in bacterial strains. Specifically, we have chosen to target SNPs that distinguish DNA from the highly pathogenic *Yersinia pestis* bacterium, the causative agent of the systemic, invasive disease commonly known as plague, from *Yersinia pseudotuberculosis*. Plague is an ancient disease that has caused three pandemics, the most recent of which is arguably still ongoing, and have resulted in the deaths of millions worldwide^{43, 44} Herein, we show that we can

successfully discriminate SNPs in a 262 bp fragment of the chaperonin encoding *groEL* and a 251 bp product of *meth* which is involved in the biosynthesis of the amino acid methionine. Discrimination was achieved using the unpurified PCR products of these targets. We show that the discrimination can be improved by conducting the experiment at a lower temperature.

Materials and methods

Identification of Single Nucleotide Polymorphisms to Distinguish *Yersinia pestis* from *Y. pseudotuberculosis*

Y. pestis specific SNPs were identified within *groEL* and *meth* using the software tool SNPs Finder.⁴⁵ Subsequently, twelve sequences for each of *groEL* and *meth* were acquired from GenBank and aligned using MegAlign ClustalW (DNASTAR Lasergene 6). A consensus sequence was exported into Primer Express v1.0 (Applied-Biosystems, UK) which was then used to design PCR primers and probes targeting discriminatory polymorphisms.

Extraction of DNA from *Y. pestis* and *Y. pseudotuberculosis*: Genomic DNA was extracted from overnight cultures of *Y. pestis* CO92 and *Y. pseudotuberculosis* NCTC 824. Genomic DNA was extracted using a QIAamp DNA mini-prep kit (Qiagen, UK) according to the manufacturer's instructions.

PCR Amplification of Templates DNA for the PCR of Labelled *groEL* and *meth* Amplicons

PCR was performed in 25 μ l reaction volumes on a GeneAmp® PCR System 9700 (Applied Biosystems, UK). Reactions contained: 0.2 μ M of forward and reverse primer, 1 \times PCR buffer without Mg^{2+} , 3 mM $MgCl_2$ (Sigma-Aldrich, UK), 80 mM each dNTP (Roche, UK), 0.04 U μ l⁻¹ Taq polymerase (Roche) and 18.4 μ l molecular grade dH₂O (Sigma-Aldrich, UK). PCR conditions were 94 °C for 5 min; 35 cycles of 95 °C for 30 s, 58 °C for 30 s and 72 °C for 30s; 72 °C 7 min. E-gels® (Invitrogen, Life Technologies, UK) were used to visualise amplicons. E-gels® were used according to the manufacturer's instructions. Visualisation was done using a Chemi HR410 BioSpectrum® Imaging System (Ultraviolet Products Ltd, UK).

Asymmetric PCR Amplification

The amplicons were amplified and labelled using asymmetric PCR. The PCR conditions were optimised for each assay by varying the concentration of the amplicons, the number of cycles and the concentration of the primers (Figures S1 and S2). The PCR reactions were performed using a thermocycler (Eppendorf Mastercycler Gradient) and they were carried out in 20 μ l volumes each containing 10 μ l of 2x BioRad SsoFast super-mix PCR master-mix and the optimised concentrations of primers and target. The amplification was monitored by adding 0.6 μ l of Sybr green (Biorad) in the reaction volume. For the *groEL* SNP assay, 0.005 pg/ μ l of double stranded DNA amplicon generated from a standard PCR amplification of the gene fragment from either *Y. pestis* or *Y. pseudotuberculosis* was used as the optimised target concentration. The primer's concentrations were 0.5 μ M for the Texas Red labelled forward primer and 0.05 μ M for the reverse primer. PCR conditions were 95 °C for 2 min, followed by 40 cycles of 95 °C for 1 s and 55 °C for 1 s. For the *meth* SNP assay, 0.5 pg/ μ l of the amplicon was used as the optimised target concentration and

the primer concentrations were 1 μ M for the Texas Red labelled forward primer and 0.1 μ M for the reverse primer. PCR conditions were 95 °C for 2 min, followed by 45 cycles of 95 °C for 1 s and 55 °C for 1 s.

Oligonucleotide Synthesis

Oligonucleotide synthesis was performed using standard methods by ATDBio Southampton, United Kingdom. This included the PCR primers and the four DNA probes (Tables 1).

Preparation of Sphere Segment Void (SSV) Substrates

A gold-chrome coated microscope slide was prepared by thermal vapour deposition of a 10 nm chromium adhesion layer followed by approximately 200 nm of gold onto a standard glass microscope slide. A monolayer template of 600 nm of polystyrene spheres (Fisher Scientific as a 1% wt aqueous suspension) was formed at the surface using a convective assembly method.³⁹ Gold was deposited through the template to a height of 480 nm at -0.72 V vs. SCE from commercial gold plating solution (ECF 60, Metalor) containing 100 μ L brightener (E3, Metalor) in 20 ml of plating solution. After deposition the polystyrene spheres were removed by immersion in DMF (Rathburn, HPLC) for thirty minutes, and the substrates were rinsed in deionised water before immediate use.

Immobilization of Probe Oligonucleotides on the Substrate and DNA Hybridization

The SSV substrates were exposed to 1 μ M probe solutions that were diluted in 10 mM Tris Buffer (pH 7.2) containing 1 M NaCl for 24 hours at room temperature. The substrates were then heated in the PCR solutions to 90 °C for 10 min and then were allowed to cool slowly to room temperature in a large water bath. This procedure improved the hybridization efficiency of the amplicon with the probes

Electrochemical Melting Procedure

Electrochemical melting experiments were carried out in a custom-built spectro-electrochemical Raman cell (Ventacon Ltd.) specifically designed for use with a Renishaw 2000 Raman microscope. It utilizes a horizontal geometry for viewing under the microscope, maintaining a thin 150 μ L liquid film on the substrate. Electrochemical control is provided by a three-electrode arrangement inside the cell, where the substrate is used as the working electrode, a platinum wire as the counter electrode, and silver/silver chloride pellet as the reference electrode. In a typical electrochemical melting experiment, the potential was swept at 0.5 mV s⁻¹ from a starting potential of 0 to -1.3 V in 10 mM Tris/1 M NaCl buffer. All electrochemical measurements were carried out using an EcoChemie AutolabIII potentiostat/galvanostat at room temperature.

Raman Instrumentation

Raman spectra were acquired using a 50 \times objective on a Renishaw 2000 microscope instrument equipped with a 632.8 nm He-Ne laser and Prior XYZ stage controller. The diameter of the laser spot was 1 μ m. Typically, Raman spectra were acquired from a 10 \times 10 μ m area with the laser moved approximately 2 μ m between measurements in order to avoid bleaching effects. The laser power was 2.3 mW and spectra were recorded with an exposure time of 30 s.

Data Analysis

SERS spectra presented were baseline-corrected using a polynomial multipoint fitting function, and curve-fitting was performed as required with Renishaw WiRe 3.1 software. The Raman intensities of the peaks are taken as height above the baseline. Origin 9.1 was used to fit sigmoidal curves to the melting profiles.

Table 1 Oligonucleotide sequences used for *groEL* SNP assay (5' to 3' combined with G1 and *metH* SNP with assays (5' to 3'). combined with probes M1, M2 and M3. Primer sequences are shown on the amplicon in bold. The position of the hybridization probe is underline and the position(s) of the mismatches are in bold and underlined.

<i>groEL</i> assay combined with probe G1	
<i>Y. pestis</i>	ATGGGGCGCACAGATGGTTAAAGAAGTTGCCTCTAAAGCAAATGATGCTGCGGGTGACGGTACCACGACTGCAACAGTATTGGCTCAATCCATCATCACTGAAGGCCTGAAAGCAGTTGCCGAGGCATGAACCAATGGATCTGAAGCGCGGCATCGACAAAGCCGTTATCGCAGCGGTAGAAGAGCTGAAAAAACTGTCTGTACCTTGCTCTGATTCCAAAGCGATTGCTCAGGTCGGTACCATCTCTGCAAACCTCCGACTC
<i>Y. pseudotuberculosis</i>	A to G at position 39bp, T to C at position 45bp
Probe G1	GCAGCATCATTTGCTTTAGAGGC-XHXHX
<i>metH</i> SNP assay combined with probe M1	
<i>Y. pestis</i>	AAATTGGGGGTACAGGTGGTGGAGGCCAGTATTGAAACTCTGCGCAACTATATCGACTGGACGCCATTCTTTATGACCTGGTCGTTGGCAGGCAAGTATCCGCGCATTTTGAAGATGAGGTGGTGGGGGAGGAGGCCAAGCGCCTGCTCGCCGACGCCAATGCTTTGTTGGATAAATTGTCCGCCGAGGATCTGCTGCATCCAAAGGCGTGTTGGTCTGTTCCCGGCTAACAGCGTCGGCGATGATAT
<i>Y. pseudotuberculosis</i>	A to G mutation at position 111bp
Probe M1	ACCTCATCTTCTAAAATGCGCGG-XHXHX
<i>metH</i> SNP assay combined with probes M2 and M3.	
<i>Y. pestis</i>	ATATCATCGCCGACGCTGTTAGCCGGGAACAGACCAACCACGCCTTTTGGATGCAGCAGATCCTCGGCGGACAATTATCCAAACAAAGCATTGGCGTCGGCGAGCAGGCGCTTGGCCTCTCCCCACCCTCATCTTCTAAAATGCGCGGATACTTGCTGCCAACGACGAGTCATAAAGAATGGCGTCCAGTCGATATAGTTGCGCAGAGTTCAATACTGGCCTCCACACCTGTACCCCCAATTT
<i>Y. pseudotuberculosis</i>	T to C mutation at position 141bp
Probe M2	CCGCGCATTTTGAAGATGAGGT-XHXHX
Probe M3	CCGCGCATTTTGAAGATGAGGT-XHXHX

(i) H=hexaethyleneglycol spacer; X=dithiol monomer

ARTICLE

Results and discussion

In this work we distinguish DNA from the highly pathogenic *Yersinia pestis* from the related *Y. pseudotuberculosis* bacterium that causes Far-East scarlet-like fever. Phylogenetic analysis by Morelli *et al.*,⁴⁶ has suggested that *Y. pestis* originated in or near China from where it was transmitted, by trade routes for example, to West Asia and Africa. It is the most virulent of the three members of the genus *Yersinia* that cause disease in humans. *Y. pestis* is a recently (~20,000 years) diverged clone of the enteric pathogen *Y. pseudotuberculosis*.⁴⁷ In contrast to the narrowed environmental reservoirs of *Y. pestis*, *Y. pseudotuberculosis* (the etiological agent of yersiniosis in animals) is a soil- and water-borne organism. In spite of this differing ecology, coupled with the marked increased virulence of *Y. pestis*, these organisms share a close genetic relationship with 2,976 chromosomal genes (75%) in *Y. pseudotuberculosis* sharing a sequence similarity to their homologues in *Y. pestis* of equal to or greater than 97%.⁴⁸ Single Nucleotide Polymorphisms (SNPs) were identified between the *Y. pestis* and *Y. pseudotuberculosis* genome. The first two SNPs were identified within a 263bp region of the *groEL* gene and consisted of an A to G polymorphism at position 38 and a T to C polymorphism at position 44 of the PCR fragment and positions 244 and 250 within the *groEL* gene respectively. The second SNP consisted of an A to G at position 111 of a 251bp fragment and position 2905 within the *metH* gene.

For both the *groEL* and *metH* assays, genomic DNA from either species was used as a template for asymmetric PCR to generate ssDNA amplicons. The DNA products, were used in their amplified, unpurified forms for hybridisation to the DNA captures probes. The capture probes were designed to be fully complementary to a 23bp section of the *Y. pestis* PCR amplicon, which overlapped the section of the *Y. pseudotuberculosis* product containing the appropriate SNPs. The capture probes were immobilised on the SSV Au surfaces prior to hybridization through three dithiol linkers to ensure that they are strongly bound to the surface. Since the DNA probes consisted of only 23bp for both assays, substantial overhanging sequences were present at both ends upon hybridization. For the *groEL* assay the two SNPs were closer to the 5' end of the amplicon which allowed most of the sequence (212bp) to overhang at the 3' end and only a short overhanging sequence (27 bases) at the 5' end. The probe (probe G1) was specifically designed in order to place the small overhanging sequence which was labelled with the Raman dye closer to the surface and to keep the longer overhanging sequence further away from the surface (Figure 1(a)). The *metH* SNP assay was much more challenging as there was only one base pair mutation in the 251bp amplicon and this was in the middle of the sequence. In this case, when the amplicon is hybridised to the probe, it has long overhanging sequences at both ends. As a result, regardless of the probe design (probe M1), the Raman label is overhanging at the end of a long ssDNA sequence (Figure 1(b)). The PCR amplicons were labelled with Texas Red during

PCR. Texas Red was chosen because it is resonant with the 633 nm excitation wavelength used in these experiments.

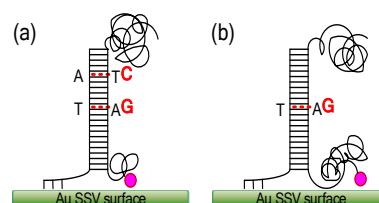


Fig. 1 Schematic representation of the immobilized PCR amplicons on the SSV surface for SNPs present in the *groEL* and *metH* assays. The red dotted lines show the positions of the base pair mismatches.

The PCR products were used without any purification and good signal to noise ratio was recorded after hybridization of the capture probes. Upon hybridization, a distinct SERS signal of the Texas Red label could be recorded for both the wild and the SNP containing amplicons for both of the assays. Some minor differences in the performance of the two assays were observed. For the *groEL* assay 0.05 μ M of the forward primer was required during PCR amplification to yield enough PCR product for sufficient hybridization of the probe. For the *metH* assay the concentration of the forward primer was doubled to yield enough PCR product to sufficiently hybridize the probe. The intensity of the Raman signal was too low when lower concentrations of the target DNA were used, indicating poor hybridization. This could be due to less accessibility of the target DNA to the capture probe due to steric crowding from the long overhanging sequences on the two sides of the complementary part of the target.

The melting experiments were carried out at high ionic strength (1M NaCl) in order to ensure that the DNA overhanging sequence that is close to the surface and labelled with the Raman dye adopts a compact conformation throughout the application of negative potentials.⁴⁹ It has been shown that in solutions of high ionic strength the DNA conformations are very robust and independent of the applied surface potential. Consequently in these conditions the DNA will coil up and remain close to the surface instead of unfolding from the surface due to repulsive electric forces. This will allow the Texas Red to be in closed proximity with the gold surface and its Raman modes to be sufficiently enhanced during the experiment.⁴⁹

Following hybridization of the probes with the PCR amplicons, the potential was ramped from a starting potential of -0.4 V to a final potential of -1.3 V vs. Ag/AgCl. Upon application of the negative potential the spectral intensities of the Texas Red bands at 1647 cm^{-1} (aromatic ring stretching) and 1504 cm^{-1} (N-H deformation) initially increased and then decreased sharply as the dsDNA on the surface started to melt. The initial increase in intensity is reversible and has been previously attributed to a change in orientation of the label with respect to the SSV surface.⁴² Figure 2 shows a typical set of

SERS spectra of Texas Red as a function of the applied potential along with a plot of the intensity of the 1504 cm⁻¹ Texas Red band as a function of potential.

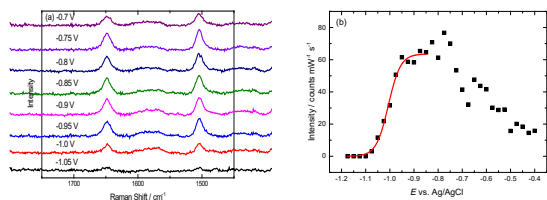


Fig. 2 (a) SERS spectra of Texas Red for the PCR fragment from *Y. Pestis* for the *groEL* assay hybridised to probe G1. The spectra have been recorded at different applied potentials vs. Ag/AgCl as shown in the figure. Spectra were acquired with 633 nm excitation laser and have been background subtracted and normalized with respect to laser power and accumulation time. The potential was swept at a scan rate of 0.5 mV s⁻¹ in 10 mM Tris buffer (pH 7.2) containing 1 M NaCl. (b) Plot of the changes in the absolute signal intensities of the band at 1504 cm⁻¹ as a function of applied potential. The red line shows the fitted electrochemical melting curve from equation 1.

Electrochemical experiments were carried out using PCR amplicons derived from both *Y. pestis* and *Y. pseudotuberculosis* for each of *groEL* and *metH* respectively. Each set of data was collected on different days, using a different batch of PCR product and a different SSV substrate in order to define the limits of the sensitivity, reliability and reproducibility of the discrimination. For each data set, the spectra were acquired at different positions on the same substrate as the electrode potential changed. Thus the scatter in the data presented here includes the effects in variation in all the stages of the assay including the preparation and uniformity of the SSV substrates, the PCR process, the hybridisation, and the electrochemical melting.

Similar to temperature melting procedures, we assume that the electrochemical melting is a two-state process, where double-stranded molecules are transferred into a single-stranded state. Then to determine the melting potentials the following sigmoidal fitting function was used

$$I = I_{\max} - \frac{I_{\max}}{(1 + \exp(\frac{E - E_m}{dE}))} \quad (1)$$

where I is the absolute spectral intensity of the band at 1504 cm⁻¹ at the applied potential E , I_{\max} is the average intensity value at the plateau for the sigmoidal curve, E_m is the melting potential when I equals $\frac{I_{\max}}{2}$, and dE is a constant that describes the sharpness of the melting curve (the gradient of the curve at E_m is $I_{\max}/4dE$). Two or three replicate experiments were carried out for each amplicon. To obtain the values for E_m and dE each individual data set was normalised by its I_{\max} value and the normalised sets of data for each amplicon were then fitted to equation (1) using a weighted global fit, where each data set was weighted in inverse proportion to its particular value of I_{\max}^2 . This gives a single common melting curve for each set of replicate experiments together with the corresponding 95% confidence interval.

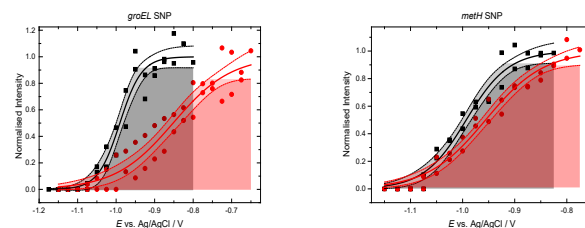


Fig. 3 Solid lines represent the electrochemical melting curves and dotted lines the 95% confidence limits, for the two amplicons, from *Y. pestis* and *Y. pseudotuberculosis* for the *groEL* and *metH* SNPs. In each case the black data corresponds to the *Y. pestis* amplicon and the red data corresponds to the *Y. pseudotuberculosis* amplicon. The *Y. pseudotuberculosis* amplicon varies from the hybridisation probe at two positions in *groEL* and one in *metH*. The potential was swept at a scan rate of 0.5 mV s⁻¹ in 10 mM Tris buffer (pH 7.2) containing 1 M NaCl.

Table 2. Melting potentials (vs. Ag/AgCl) and dE values for the *groEL* amplicons bound to probe G1 and *metH* amplicons bound to probe M1 determined from the global fitting of the two data set collected for each amplicon to equation 1

	<i>Y. pestis</i>	<i>Y. pseudotuberculosis</i>
E_m (<i>groEL</i>) / V	-0.99±0.006	-0.852±0.021
dE (<i>groEL</i>) / V	0.028±0.005	0.075±0.013
E_m (<i>metH</i>) / V	-0.993±0.007	-0.956±0.009
dE (<i>metH</i>) / V	0.041±0.005	0.056±0.006

Figure 3 shows the two electrochemical melting curves, for the two amplicons, from *Y. pestis* (fully complementary) and *Y. pseudotuberculosis* (containing the SNPs), for the *groEL* and *metH* assays respectively. In this case two replicate experiments were performed at room temperature (~20°C) and the 95% confidence intervals were plotted along with the sigmoidal curves. The width of the confidence interval is proportional to the standard error of the predicted I value. It is obvious from the figures that, taking into account of the 95% confidence intervals, discrimination of the SNPs has been achieved for both assays. The E_m and dE values are given in Table 2. The discrimination is significantly better for the *groEL* SNPs compared to that for the *metH* SNP. This is expected since in the case of the *groEL* there are two mismatches in the *Y. pseudotuberculosis* sequence. In addition, the melting curve of the amplicon from *Y. pestis* containing no SNPs is significantly steeper compared to that of the amplicon containing the polymorphism. More specifically dE was calculated to be 28 mV for the wild type and 75 mV for the SNPs. This was due to the stability of the perfectly matched duplex which is essentially higher than the mismatched sequence. *Y. pestis* and *Y. pseudotuberculosis* could still be discriminated using the *metH* assay, however both strands displayed broad melting profiles which rendered the discrimination poor under these conditions.

Electrochemical melting at 10 °C

One powerful advantage of the electrochemical melting technique is that we can combine control of the experimental temperature with the electrochemical potential to denature DNA sequences. It is expected that at lower temperatures DNA sequences will be more stable and therefore the difference in the melting potential between the perfect and mismatched amplicon will be more pronounced. The experimental temperature was therefore decreased to 10 °C in order to improve the discrimination for the *metH* assay. In addition, to

further explore the ability of this technique to discriminate single base mismatches in long DNA strands experiments were carried out to discriminate the *metH* SNP when it is present on the complementary DNA strand of the *Y. pestis* or *Y. pseudotuberculosis* PCR amplicon. To do this two additional probes were designed, probe M2 that is complementary to *Y. pestis* and probe M3 is that complementary to *Y. pseudotuberculosis*.

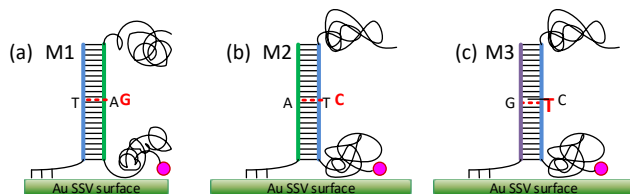


Fig. 4 Representation of the immobilization of the *metH* PCR amplicons on the SSV surface hybridised to probes M1, M2 and M3 respectively. The red dotted lines show the positions of the base mismatches for each probe.

Figure 4 shows a schematic representation of the three combinations of mismatches for the *metH* assay. Probe M1 (Figure 4(a)) is fully complementary with a 23 bp section of the *Y. pestis* PCR amplicon, that overlaps the section of the *Y. pseudotuberculosis* amplicon containing the appropriate SNP. When probe M1 is hybridised with the PCR amplicons there is a 99bp sequence that overhangs at the bottom of the 23bp hybridized section, close to the surface, and a 129bp sequence that overhangs at the top of the hybridized section. Hybridization of probe M1 with the *Y. pseudotuberculosis* PCR amplicon yields to a T-G mismatch at position 111 that needs to be discriminated against a T-A match (where the first base refers to the probe). When probe M2 is used (Figure 4(b)), the probe is reversed with the target. In this case, the primers used to amplify and label the ssDNA amplicon for hybridisation were substituted to generate a different product in the opposite orientation. As for probe M1, probe M2 is fully complementary to a 23bp section of the *Y. pestis* PCR amplicon, that overlaps the section of the *Y. pseudotuberculosis* product containing the appropriate SNP. Hybridization of probe M2 with *Y. pseudotuberculosis* yields an A-C mismatch at position 140 of the amplicon that needs to be discriminated against an A-T match. In the last case (Figure 4(c)), the PCR amplicon is the same as when probe M2 was utilised but the probe, probe M3, is changed to be complementary to a 23bp section of the *Y. pseudotuberculosis* amplicon. Hybridization of probe M3 with *Y. pestis* yields a G-T mismatch at position 140 of the amplicon that needs to be discriminated against a G-C match. Upon hybridization of the PCR amplicons to either probe M2 or M3, a 129bp sequence overhangs at the bottom of the hybridised 23bp section, close to the surface and a 99bp sequence overhangs at the top in contrast to M1 where the lengths of the two overhangs are reversed.

Table 2. Experimental melting temperatures for the probes M1, M2 and M3 hybridised with the 23 base long perfectly complementary and mismatched synthetic targets.

	Perfect match	Mismatch
T_m probe M1 / °C	76.97±0.15	73.43±0.14
T_m probe M2 / °C	76.35±0.11	70.41±0.19
T_m probe M3 / °C	73.53±0.13	78.65±0.11

The electrochemical melting experiments were carried out at 10 °C as the discrimination efficiency was expected to be improved at lower temperatures. Three replicates have been carried out for each amplicon and, as in the earlier experiments, each data set was collected on different days, using different batches of PCR products and SSV substrates. The three replicate sets of data were analysed as described above. The results are plotted in Figure 5 for each amplicon and for each probe; Table 4 summarises the E_m and dE values. It is clear from the figure that the two amplicons are clearly discriminated for all the cases and in all the repeats. UV melting experiments have been carried out using similar conditions to the electrochemical melting experiments (10 mM Tris Buffer, 1 M NaCl) and the results are given in Table 3.

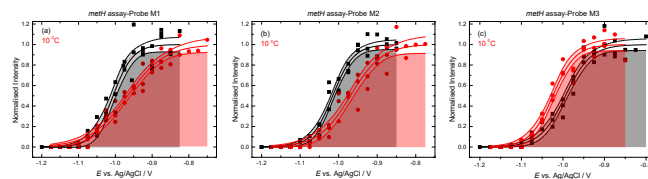


Fig. 5 Solid lines represent the electrochemical melting curves and dotted lines the 95% confidence limits, for the two amplicons, from *Y. pestis* and *Y. pseudotuberculosis* for the *metH* SNPs hybridised to probes M1, M2 and M3 respectively. In each case the black data corresponds to the *Y. pestis* amplicon and the red data corresponds to the *Y. pseudotuberculosis* amplicon. The *Y. pseudotuberculosis* amplicon varies from the hybridisation probe one in positions. The potential was swept at a scan rate of 0.5 mV s⁻¹ in 10 mM Tris buffer (pH 7.2) containing 1 M NaCl. The experiment has been conducted at 10 °C.

Table 4. Melting potentials (vs. Ag/AgCl) and dE values for the *metH* amplicons bound to probes M1, M2 and M3 respectively, determined from the global fitting of the two data set collected for each amplicon to equation 1. The experiments have been conducted at 10 °C.

	<i>Y. pestis</i>	<i>Y. pseudotuberculosis</i>
E_m (probe M1) / V	-1.006±0.005	-0.967±0.006
dE (probe M1) / V	0.027±0.004	0.051±0.005
E_m (probe M2) / V	-1.015±0.003	-0.970±0.007
dE (probe M2) / V	0.027±0.003	0.041±0.005
E_m (probe M3) / V	-0.994±0.004	-1.024±0.004
dE (probe M3) / V	0.031±0.003	0.027±0.003

Figures 5(a) and (b) show discrimination of the two amplicons utilising the probes M1 and M2 that are fully complementary to *Y. pestis* amplicons. Upon hybridization of either probe M1 or M2 to *Y. pestis*, the perfect match remains the same (T-A or A-T) as the two sequences (probe and target) are reversed. Even though the two E_m values are very similar i.e. -1.006 V when probe M1 was utilised and -1.015 V when probe M2 was utilised, they are not identical. This can be attributed to the subtle differences in the design of the experiments such as the difference in the length of the overhangs in the target sequence for each case as well as the position of the mismatch in the amplicon. Interestingly, the melting transition of the perfectly matched sequence was very similar for both probes, with a similar dE in both cases (Figure 6) demonstrating the robustness of the method. The melting transitions for both the mismatched sequences remain broad. The UV melting studies showed that the T-G mismatch ($T_m \sim 73.53$ °C) upon

hybridization of probe M1 with *Y. pseudotuberculosis* is slightly more stable compare to the A-C mismatch ($T_m \sim 70.41^\circ\text{C}$) upon hybridization of probe M2 to the same amplicon. Improved discrimination is therefore expected when the probe M2 is used. Indeed, there is a slight improvement, more precisely there is a 45 mV difference between the E_m values of the *Y. pestis* and *Y. pseudotuberculosis* when probe M2 was utilised against 39 mV when probe M1 was utilised. However this improvement is not strongly significant when you take into account the confidence intervals, suggesting that the method is not very sensitive to these subtle differences. We note that because of the differences in dE , for both of these experiments there is better discrimination at the potential at which $\sim 70\%$ of the oligonucleotide has melted.

Figure 5(c) shows discrimination of the two amplicons utilising the probe M3 that is fully complementary to the *Y. pseudotuberculosis* amplicon, where the perfect G-C match ($T_m \sim 78.65^\circ\text{C}$) was discriminated against a G-T mismatch ($T_m \sim 73.53^\circ\text{C}$). The E_m of the perfectly matched sequence is higher compared to the corresponding values of the perfect duplexes when M1 and M2 were utilised (Table 3), which agrees with the results from the melting studies (Table 2). This is due to the G-C match being thermodynamically more stable than the T-A/A-T matches. It should also be noted that the melting curves were steep (smaller dE) for both the perfect match and mismatch duplexes for this probe.

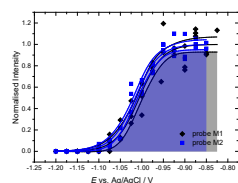


Fig. 6 Electrochemical melting curves for the perfectly matched duplexes for the probes M1 and M2. Three replicate sets for data have been collected for each duplex. The data were combined after normalization and were fitted to equation 1. The potential was swept at a scan rate of 0.5 mV s^{-1} in 10 mM Tris buffer (pH 7.2) containing 1 M NaCl at 10°C .

Irrespective of above considerations, we have shown that discrimination of single base mismatches in long unpurified PCR products is possible and reproducible with all three different probes, demonstrating that electrochemical DNA melting is a powerful DNA platform that can be implemented in important practical applications. There are several notable features of the combination of electrochemical melting and SERS detection that make this method particularly robust. First we use the SSV substrates to achieve the SERS enhancement. These surfaces are sculpted to achieve the required plasmonic enhancement of the SERS at both the incoming and outgoing wavelengths. Importantly the SSV surface is not rough but rather smooth and reproducible on the nanoscale having a relatively low (around 4 times the projected geometric) surface area. It is also stable with respect to changes in electrode potential. Second we scan the potential, to bring about melting of the dsDNA, but use the SERS as the output signal rather than electrochemical measurement (current, capacitance, etc.) that might be distorted by interference from other processes. Third, because we use SERS we are able to use the characteristic molecular vibrations of the label and thus discriminate against any interferences from other molecules at the electrode surface. This also means that it is possible to multiplex the measurement by using combinations of Raman labels. Fourth, the surface

enhancement is strongly distance dependent such that the signal for the labelled dsDNA is enhanced by around 10^9 relative to that for molecules in solution. Consequently we do not need to use washing steps and can perform the discrimination in the unpurified PCR buffer. Fifth, the discrimination depends on following the denaturation and identifying the potential at which the signal falls to some predetermined fraction of the original value. Thus the absolute amount of target DNA hybridised on the surface does not matter provided it is sufficient to give clear spectra. Finally the potential is a sensitive and easily measured parameter. As a consequence of these features the method is also highly sensitive. In the, non-optimised experiments reported here we have shown discrimination of the SNP from 4 μl of starting solutions of 0.3 pM *groEL* (0.0012 fmols of DNA) and 30 pM *metH* (0.12 fmols of DNA) in a total time of ~ 105 min for PCR amplification, hybridisation to the surface bound probe and electrochemical melting.

Conclusions

For the first time it has been possible to use SERS and electrochemical melting to reliably demonstrate the discrimination of nucleotide polymorphisms in long ($>250\text{bp}$) PCR amplicons with no requirement for additional purification or preparation steps. Genomic DNA was extracted from *Y. pestis* and *Y. pseudotuberculosis* and amplified and labelled using conventional PCR; importantly the PCR products were used unpurified. This represents a realistic real world test for DNA hybridisation sensors of this type. This is the first example of the discrimination of nucleotide polymorphisms in PCR amplicons of this length for any SERS-based DNA sensor. Two assays targeting SNPs that exist between gene targets present on the chromosome of *Y. pestis* and *Y. pseudotuberculosis* have been presented. The first; targeting *groEL*, has two single base mismatches and the second one targeting *metH* has only one base mismatch. Both assays represent a substantial step forward in proving the application of this approach to DNA detection and discrimination of closely related DNA products and show that the length of the DNA products does not hamper the performance of the approach due to steric issues of the labelled DNA close to the sensor surface. The *metH* SNP assay was significantly more challenging than the *groEL* assay both in terms of the presence of only one nucleotide mismatch and the presence of the mutation in the middle of the long PCR amplicon. The technical challenge posed by this amplicon was successfully overcome by reducing the experimental temperature to 10°C to improve the discrimination, these conditions were employed to successfully detect three different combinations of mismatch utilizing three different probes. Replicate data were collected for each probe/target duplex on different days, using different batches of PCR product and different SSV substrates; the results clearly demonstrate the sensitivity and reliability of the discrimination. The performance of the assays and the measurement strategy has been shown to be highly reliable and robust. The proposed DNA assay which combines electrochemistry with SERS and coupled with PCR, has a significant potential to approach problems with real life application.

Acknowledgements

EP acknowledges the Ministry of Defence of the funding

Notes and references

^a Chemistry, University of Southampton, Highfield, Southampton, SO17 1BJ

^b DSTL, Porton Down, Salisbury, Wiltshire SP4 0JQ.

^c ATDBio Ltd, Chemistry, University of Southampton, Highfield, Southampton, SO17 1BJ

^d Department of Chemistry, University of Oxford, Chemistry Research Laboratory, Oxford OX1 3TA

Electronic Supplementary Information (ESI) available: [PCR amplification curves for different concentrations of the *Y. pestis* and *Y. pseudotuberculosis* amplicons for the *groEL* and *metH* assays., experimental details for the UV melting studies]. See DOI: 10.1039/b000000x/

1. C. R. Taitt, A. P. Malanoski, B. Lin, D. A. Stenger, F. S. Ligler, A. W. Kusterbeck, G. P. Anderson, S. E. Harmon, L. C. Shriver-Lake, S. K. Pollack, D. M. Lennon, F. Lobo-Menendez, Z. Wang and J. M. Schnur, *FEMS Immunol. Med. Microbiol.*, 2008, **54**, 356.
2. P. E. Granum and T. Lund, *FEMS Microbiol. Lett.*, 1997, **157**, 223.
3. K. K. Amoako, M. C. Thomas, F. Kong, T. W. Janzen, K. R. Hahn, M. J. Shields and N. Goji, *J. Microbiol. Methods*, 2012, **90**, 228.
4. A. Lermo, E. Zacco, J. Barak, M. Delwiche, S. Campoy, J. Barbe, S. Alegret and M. I. Pividori, *Biosens. Bioelectron.*, 2008, **23**, 1805.
5. T. D. Minogue, P. A. Rachwal, A. Trombley Hall, J. W. Koehler and S. A. Weller, *Appl. Environ. Microbiol.*, 2014, **80**, 1322.
6. S. A. Weller, V. Cox, A. Essex Lopresti, M. G. Hartley, T. M. Parsons, P. A. Rachwal, H. L. Stapleton and R. A. Lukaszewski, *J. Med. Microbiol.*, 2012, **61**, 1546.
7. C. T. Wittwer, M. G. Herrmann, C. N. Gundry and K. S. J. Elenitoba-Johnson, *Methods*, 2001, **25**, 430.
8. J. Z. Song, Q. Yang, F. T. Lv, L. B. Liu and S. Wang, *ACS Appl. Mater. Interfaces*, 2012, **4**, 2885.
9. D. J. French, C. L. Archard, T. Brown and D. G. McDowell, *Mol. Cell. Probes*, 2001, **15**, 363-374.
10. K. Faulds, W. E. Smith and D. Graham, *Anal. Chem.*, 2004, **76**, 412.
11. D. van Lierop, K. Faulds and D. Graham, *Anal. Chem.*, 2011, **83**, 5817.
12. D. Graham, B. J. Mallinder, D. Whitcombe, N. D. Watson and W. E. Smith, *Anal. Chem.*, 2002, **74**, 1069.
13. H.-N. Wang and T. Vo-Dinh, *Nanotechnology*, 2009, **20**.
14. E. M. Boon, D. M. Ceres, T. G. Drummond, M. G. Hill and J. K. Barton, *Nat. Biotechnol.*, 2000, **18**, 1096.
15. G. Carpinì, F. Lucarelli, G. Marrazza and M. Mascini, *Biosens. Bioelectron.*, 2004, **20**, 167.
16. G. Marrazza, G. Chiti, M. Mascini and M. Anichini, *Clin. Chem.*, 2000, **46**, 31.
17. D. Ozkan, A. Erdem, P. Kara, K. Kerman, B. Meric, J. Hassmann and M. Ozsoz, *Anal. Chem.*, 2002, **74**, 5931.
18. B. Meric, K. Kerman, D. Ozkan, P. Kara, S. Erensoy, U. S. Akarca, M. Mascini and M. Ozsoz, *Talanta*, 2002, **56**, 837.
19. P. Kara, C. Cavusoglu, S. Cavdar and M. Ozsoz, *Biosens. Bioelectron.*, 2009, **24**, 1796.
20. S. Aydinlik, D. Ozkan-Ariksoysal, P. Kara, A. A. Sayiner and M. Ozsoz, *Anal. Methods*, 2011, **3**, 1607.
21. Fleischmann, P. J. Hendra and McQuillan, *Chem. Phys. Lett.*, 1974, **26**, 163.
22. C. L. Haynes, A. D. McFarland and R. P. Van Duyne, *Anal. Chem.*, 2005, **77**, 338A.
23. E. Papadopolou and S. E. J. Bell, *Chem. Eur. J.*, 2012, **18**, 5394.
24. E. Papadopolou and S. E. J. Bell, *Angew. Chem. Int. Ed.*, 2011, **50**, 9058.
25. A. Barhoumi, D. Zhang, F. Tam and N. J. Halas, *J. Am. Chem. Soc.*, 2008, **130**, 5523.
26. D. Graham and K. Faulds, *Chem. Soc. Rev.*, 2008, **37**, 1042.
27. T. Vo-Dinh, H.-N. Wang and J. Scaffidi, *J. Biophotonics*, 2010, **3**, 89.
28. C. Feuillie, M. M. Merheb, B. Gillet, G. Montagnac, C. Haenni and I. Daniel, *Anal. Bioanal. Chem.*, 2012, **404**, 415.
29. A. MacAskill, D. Crawford, D. Graham and K. Faulds, *Anal. Chem.*, 2009, **81**, 8134.
30. P. B. Monaghan, K. M. McCarney, A. Ricketts, R. E. Littleford, F. Docherty, W. E. Smith, D. Graham and J. M. Cooper, *Anal. Chem.*, 2007, **79**, 2844.
31. L. Sun and J. Irudayaraj, *J. Phys. Chem. B*, 2009, **113**, 14021.
32. P. N. Bartlett, J. J. Baumberg, P. R. Birkin, M. A. Ghanem and M. C. Netti, *Chem. Mater.*, 2002, **14**, 2199.
33. S. Mahajan, J. J. Baumberg, A. E. Russell and P. N. Bartlett, *Phys. Chem. Chem. Phys.*, 2007, **9**, 6016.
34. S. Cintra, M. E. Abdelsalam, P. N. Bartlett, J. J. Baumberg, T. A. Kelf, Y. Sugawara and A. E. Russell, *Faraday Discuss.*, 2006, **132**, 191.
35. T. A. Kelf, Y. Sugawara, J. J. Baumberg, M. Abdelsalam and P. N. Bartlett, *Phys. Rev. Lett.*, 2005, **95**, 116802.
36. R. M. Cole, J. J. Baumberg, F. J. Garcia de Abajo, S. Mahajan, M. Abdelsalam and P. N. Bartlett, *Nano Lett.*, 2007, **7**, 2094.
37. R. G. Sosnowski, E. Tu, W. F. Butler, J. P. Oconnell and M. J. Heller, *Proc. Natl. Acad. Sci. U.S.A.*, 1997, **94**, 1119.
38. V. Brabec and E. Palecek, *Biophys. Chem.*, 1976, **4**, 79.
39. S. Mahajan, J. Richardson, T. Brown and P. N. Bartlett, *J. Am. Chem. Soc.*, 2008, **130**, 15589.
40. R. P. Johnson, R. Gao, T. Brown and P. N. Bartlett, *Bioelectrochemistry*, 2012, **85**, 7.
41. R. P. Johnson, J. A. Richardson, T. Brown and P. N. Bartlett, *J. Am. Chem. Soc.*, 2012, **134**, 14099-14107.
42. D. K. Corrigan, N. Gale, T. Brown and P. N. Bartlett, *Angew. Chem. Int. Ed.*, 2010, **49**, 5917.
43. R. D. Perry and J. D. Fetherston, *Clin. Microbiol. Rev.*, 1997, **10**, 35.
44. S. Riedel, *Proc. (Bayl. Univ. Med. Cent.)*, 2005, **18**, 116.
45. J. Song, Y. Xu, S. White, K. W. P. Miller and M. Wolinsky, *Bioinformatics*, 2005, **21**, 2083.
46. G. Morelli, Y. Song, C. J. Mazzoni, M. Eppinger, P. Roumagnac, D. M. Wagner, M. Feldkamp, B. Kusecek, A. J. Vogler, Y. Li, Y. Cui, N. R. Thomson, T. Jombart, R. Leblois, P. Lichtner, L. Rahalison, J. M. Petersen, F. Balloux, P. Keim, T. Wirth, J. Ravel, R. Yang, E. Carniel and M. Achtman, *Nat. Genet.*, 2010, **42**, 1140.
47. M. Achtman, K. Zurth, C. Morelli, G. Torrea, A. Guiyoule and E. Carniel, *Proc. Natl. Acad. Sci. U.S.A.*, 1999, **96**, 14043.
48. P. S. G. Chain, E. Carniel, F. W. Larimer, J. Lamerdin, P. O. Stoutland, W. M. Regala, A. M. Georgescu, L. M. Vergez, M. L. Land, V. L. Motin, R. R. Brubaker, J. Fowler, J. Hinnbusch, M. Marceau, C. Medigue, M. Simonet, V. Chenal-Francisque, B. Souza, D. Dacheux, J. M. Elliott, A. Derbise, L. J. Hauser and E. Garcia, *Proc. Natl. Acad. Sci. U.S.A.*, 2004, **101**, 13826.
49. W. Kaiser and U. Rant, *J. Am. Chem. Soc.*, 2010, **132**, 7935.